POLITECNICO
MILANO 1863

SCUOLA DI INGEGNERIA INDUSTRIALE
E DELL'INFORMAZIONE

Executive Summary of the Thesis

Inter-Satellite Link based Relative Navigation for Spacecraft Formation Flying

Laurea Magistrale in Space Engineering - Ingegneria Spaziale

Author: Francesco De Cecio

Advisor: Prof. Michèle Roberta Lavagna

Co-advisor: Dott. Stefano Silvestrini

Academic year: 2021-2022

1. Introduction

Spacecraft formation flying missions are becoming more and more popular in the current years for different reasons. First, distributed systems allow for increasing the missions' scientific return and reducing the overall costs. Moreover, they enable interferometric, stereoscopic and SAR imaging techniques with unprecedentedly large baselines.

Both large formations in Earth orbit or deep-space one fall beyond the capabilities of the traditional ground-based control scheme. For this reason, it is essential to provide a communication channel between the platforms by optical or RF inter-satellite link (ISL) that allows autonomous formation maintenance.

While the performances of the optical ISL are extremely promising, it is still challenging to implement them on low-budget missions since they require more sophisticated devices and very accurate pointing. RF solutions are instead cheap and reliable enough to be considered in almost all mission classes, albeit being characterised by lower performances [1].

This thesis explores the techniques currently available for performing RF ISL-based relative navigation in a CubeSat formation.

2. Objectives

This thesis has three main objectives:

1. Provide an overview of the available ISL-based ranging methods and discuss their applicability to relative navigation algorithms;
2. Present the mathematical models of the more promising ISL-based ranging techniques and identify what are the errors that affect their accuracy;
3. Assess the accuracy of the selected approaches within a navigation filter to understand their impact on both absolute and relative navigation.

These objectives are addressed with a critical literature review and with numerical simulations. These latter have been performed in a framework that allows high-fidelity simulation of the ground-truth dynamics and its comparison with the estimated states from an absolute and relative standpoint.

3. Ranging techniques

Inter-satellite ranging methods can be categorized into two main families: direct and indirect methods [1].

Indirect methods exploits ISL only for exchanging absolute measurements between the platforms. There is no active role of the RF signals in the measurement process, but they are only used as a communication channel. In this case, the relative measurements are obtained by subtracting two absolute measurements. These latter shall be brought, in turn, from external systems like GNSS or ground station tracking.
Direct methods actively exploit the signal to measure the distance between the transmitting and receiving spacecraft. Generally, distance can be inferred from time or phase measurements made on the signal. They have the advantage of being independent of external systems, enabling fully-autonomous relative navigation. Moreover, higher accuracy levels can be reached by adopting this strategy. Depending on the adopted measurement scheme, they are further classified into one and two-way ranging methods.
Considering flight heritage, robustness and theoretical performances, an indirect and a direct technique have been selected and modelled. These are indirect ranging based on the exchange of absolute GNSS positions and velocities via ISL and a direct one-way GNSS-like ranging. This latter uses a signal with the same structure as the one used by GNSS constellations but locally generated onboard. The receiver spacecraft can process this signal to retrieve the inter-satellite distance from the two classical observables: pseudorange and carrier-phase.
The measurement models for the proposed techniques are reported in the following paragraphs.

Indirect ranging model To model this technique, it has been assumed that each spacecraft transmits a message, including position and velocity vectors (ECI frame) and measurement timestamp, to its companion.
Only the measurements from spacecraft A are reported for conciseness.

$$GNSS_A = \begin{bmatrix} \mathbf{r}_A^{ECI} \\ \mathbf{v}_A^{ECI} \\ t \end{bmatrix} + \begin{bmatrix} \mathbf{w_r} \\ \mathbf{w_v} \\ w_t \end{bmatrix} \tag{1}$$

$$\begin{aligned} \mathbf{w}_{\mathbf{r},\mathbf{v}} &\sim \mathcal{N}_3(\mathbf{0},\, \mathbf{\Sigma}_{\mathbf{r},\mathbf{v}}) \\ w_t &\sim \mathcal{N}_1(0,\, \sigma_t^2) \end{aligned} \tag{2}$$

A transmission delay always exists between measurement collection and usage by the navigation filter. Considering the onboard relative navigation filter of spacecraft A, it will only have access to spacecraft B's measurements at the time expressed in Eq. (3).

$$t_{RX} = t_{TX} + \Delta t_{BA}^{trn} \tag{3}$$

This delay is the sum of several factors involved in signal transmission: the geometrical time-of-flight, the ionospheric delay, and the line bias.

$$\Delta t_{BA}^{trn} = \delta t_{BA}^{tof} + \delta t_{BA}^{ion} + \delta t_A^{ln} \tag{4}$$

$$\delta t_{BA}^{tof} = \frac{|\mathbf{r}_A(t) - \mathbf{r}_B(t - \Delta t_{BA}^{trn})|}{c} \tag{5}$$

$$\delta t_{BA}^{ion} = \frac{40.3}{c\, f^2}\, TEC_{BA} \tag{6}$$

Where c is the speed of light in vacuum, f is the carrier frequency, and TEC is the ionospheric Total Electron Content on the signal's propagation path, which has been computed with the International Reference Ionosphere model. Line bias δt_A^{ln} is the time required from the signal's arrival at the receiving antenna to its complete decoding.

GNSS-like direct ranging model A measurement model for both observables has been derived based on a modified version of the model proposed by Psiaki for CDGPS [2]. Pseudorange and carrier-phase have been modelled by Eq. (7) and Eq. (8).

$$\begin{aligned} \rho_{BA}(t) &= |\mathbf{r}_A(t) - \mathbf{r}_B(t - \Delta t_{BA}^{trn})| \\ &\quad + c\,(\delta t_A - \delta t_B) + c\,\delta t_{BA}^{ion} + c\,\delta t_A^{ln} + \varepsilon_\rho^{th} \end{aligned} \tag{7}$$

$$\begin{aligned} \Phi_{BA}(t) &= |\mathbf{r}_A(t) - \mathbf{r}_B(t - \Delta t_{BA}^{trn})| \\ &\quad + c\,(\delta t_A - \delta t_B) + \lambda\,(\gamma_A^0 - \psi_B^0) - c\,\delta t_{BA}^{ion} \\ &\quad + c\,\delta t_A^{ln} - \lambda\,(\delta\phi_{\mathrm{A}}^{\mathrm{pwu}} + \delta\phi_{\mathrm{A}}^{\mathrm{mp}} + \delta\phi_{\mathrm{A}}^{\mathrm{pc}} + \varepsilon_\phi^{th}) \end{aligned} \tag{8}$$

Where $\varepsilon_{\rho,\phi}^{th}$ are the receiver's thermal noises whose standard deviation is given by design parameters. Furthermore, $\delta\phi_{\mathrm{A}}^{\mathrm{pwu}}$, $\delta\phi_{\mathrm{A}}^{\mathrm{mp}}$, $\delta\phi_{\mathrm{A}}^{\mathrm{pc}}$ are the perturbations due to phase windup, signal's multipath, and antenna phase-centre deviation. The fourth term of Eq. (8) represents the carrier-phase ambiguity. It is entirely arbitrary and

changes whenever the tracking is lost. For this reason, there is no way to estimate its value from carrier-phase measurements only. Albeit the estimation of this ambiguity is somehow challenging, once this is achieved, carrier-phase measurements can reach *cm* to *mm* accuracy.
It shall be considered that this system can operate without GNSS coverage (and thus without its time corrections). In this scenario, onboard clocks drift rapidly due to their frequency instability, causing potentially unbounded errors. The well-known two-state clock error model has been used to evaluate the clock biases $\delta t_{A,B}$ [3].

4. Navigation filter

After reviewing all the ranging techniques and selecting the most promising ones for a CubeSat application, an implementation of their measurement models within an **Extended Kalman Filter for a two-spacecraft formation** is now proposed. Although many alternatives are possible, the intention is to create a simple and versatile tool that can be used, through appropriate simulations, to assess the performances of different navigation strategies.

Time update The filter's dynamics is expressed by an absolute-based nonlinear model expressed in the ECI frame. The equations of motion are those from the unperturbed two-body problem, with the addition of empirical accelerations in a reduced-dynamics approach.

$$\ddot{\mathbf{r}} = -\frac{\mu}{\mathrm{r}^3}\,\mathbf{r} + \mathbf{a}^{\mathrm{emp}} \tag{9}$$

The state vector is hence in the form:

$$\mathbf{x}_{\mathrm{abs}} = \left\{\mathbf{r}_A, \mathbf{v}_A, \mathbf{a}_A^{\mathrm{emp}}, \mathbf{r}_B, \mathbf{v}_B, \mathbf{a}_B^{\mathrm{emp}}\right\}^T_{\mathrm{ECI}} \tag{10}$$

Once the absolute state is known, it is possible to obtain the relative one by difference. This latter is expressed in the LVLH frame.
The nonlinear state transition function can be written as follows, while the stochastic part of the state, namely the empirical accelerations, is treated as a first-order Gauss-Markov process.

$$\begin{aligned}\hat{\mathbf{x}}_k^{(-)} &= \mathcal{F}\left(\hat{\mathbf{x}}_{k-1}^{(+)}\right) = \\ &= \hat{\mathbf{x}}_{k-1}^{(+)} + \int_{t_{k-1}}^{t_k} \dot{\mathbf{x}}\left(\hat{\mathbf{x}}_{k-1}^{(+)}, \tau\right) d\tau\end{aligned} \tag{11}$$

$$\mathbf{a}_k^{\mathrm{emp}} = m(\Delta t)\,\mathbf{a}_{k-1}^{\mathrm{emp}} = e^{-\frac{\Delta t}{\tau}}\,\mathbf{a}_{k-1}^{\mathrm{emp}} \tag{12}$$

The covariance update is performed with a first-order linearization of the dynamics.

$$\boldsymbol{F}_{k-1} = \left.\frac{\partial \mathcal{F}}{\partial \mathbf{x}}\right|_{\hat{\mathbf{x}}_{k-1}^{(+)}} = \boldsymbol{I} + \Delta t \left.\frac{\partial \dot{\mathbf{x}}}{\partial \mathbf{x}}\right|_{\hat{\mathbf{x}}_{k-1}^{(+)}} \tag{13}$$

$$\boldsymbol{P}_k^{(-)} = \boldsymbol{F}_{k-1}\boldsymbol{P}_{k-1}^{(+)}\boldsymbol{F}_{k-1}^T + \boldsymbol{Q} \tag{14}$$

Where $\boldsymbol{Q}$ is the process noise covariance matrix of the proposed EKF. In this design, only the empirical accelerations have an associated process noise in the following form, while the terms for deterministic states are set to zero.

$$q_a = \sigma_a^2\left(1 - m^2(\Delta t)\right) \tag{15}$$

Measurement update The GNSS receivers onboard both spacecraft periodically produce a measurement package structured as the one modelled by Eq. (1). While the measurements taken by GNSS receiver A are available immediately, those of GNSS receiver B will be available after an amount of time equal to the transmission delay, quantified by Eq. (4). For this reason, assuming that both receivers output their navigation solution at the same instant, which is also synchronized with a filter's update, only the measurement from A will be available for processing at that iteration. Those from B will be processed at the subsequent iteration, introducing an error since spacecraft B will keep moving during this waiting time.
Denoting with the subscript G the GNSS-related quantities, the state's measurement update is:

$$\hat{\mathbf{x}}_k^{(+)} = \hat{\mathbf{x}}_k^{(-)} + \boldsymbol{K}_{G\,k}\left[\mathbf{y}_{G\,k} - \boldsymbol{H}_G\,\hat{\mathbf{x}}_k^{(-)}\right] \tag{16}$$

Where $\mathbf{y}_{G\,k} = GNSS_{A,B\,k} = \begin{bmatrix}\mathbf{r}_{A,B}^{ECI} \\ \mathbf{v}_{A,B}^{ECI}\end{bmatrix}_{t_k}$

$$\boldsymbol{H}_{G_A} = [\boldsymbol{I}_{6\times 6}\,,\ \boldsymbol{0}_{6\times 12}]$$
$$\boldsymbol{H}_{G_B} = [\boldsymbol{0}_{6\times 9}\,,\ \boldsymbol{I}_{6\times 6}\,,\ \boldsymbol{0}_{6\times 3}]$$

Since this measurement update is linear with respect to the state, the observation matrices are constant. Finally, the state covariance update is performed in Joseph's form, characterized by better numerical properties.

$$\begin{aligned}\boldsymbol{P}_k^{(+)} = &\left[\boldsymbol{I} - \boldsymbol{K}_{G\,k}\boldsymbol{H}_G\right]\boldsymbol{P}_k^{(-)}\left[\boldsymbol{I} - \boldsymbol{K}_{G\,k}\boldsymbol{H}_G\right]^T \\ &+ \boldsymbol{K}_{G\,k}\,\boldsymbol{R}_G\,\boldsymbol{K}_{G\,k}^T\end{aligned} \tag{17}$$

For GNSS measurements, the covariance matrix reads:

$$\boldsymbol{R}_G = \begin{bmatrix} \boldsymbol{\Sigma}_{\mathbf{r}} & \mathbf{0}_{3\times3} \\ \mathbf{0}_{3\times3} & \boldsymbol{\Sigma}_{\mathbf{v}} \end{bmatrix} \tag{18}$$

Where the block diagonal entries are the position and velocity covariance matrices of the employed GNSS receiver.

Inter-Satellite pseudoRange (ISR) measurements can be obtained in almost real-time and at a higher rate than GNSS ones. In this case, the measurement update function is nonlinear and it needs to be linearized at each iteration around the current estimate to compute the observation matrix. However, an analytical expression for the Jacobian can be employed to reduce the computational burden. The derivation starts by writing the nonlinear measurement function employed in the filter:

$$\hat{y}_\rho = h\left(\hat{\mathbf{x}}\right) = \left[\mathbf{r}_B - \mathbf{r}_A\right]^T \left[\mathbf{r}_B - \mathbf{r}_A\right] \tag{19}$$

The inter-satellite distance is taken squared inside the function to make vanish the square root associated with distance computation. The desired Jacobian reads:

$$\boldsymbol{H}_{\rho\,k} = \left.\frac{\partial h}{\partial \mathbf{x}}\right|_{\hat{\mathbf{x}}_k^{(-)}} = 2\Delta\hat{\mathbf{r}}_k^{(-)T}\left[-\boldsymbol{I}_{3\times3}\,,\ \mathbf{0}_{3\times6}\,,\ \boldsymbol{I}_{3\times3}\,,\ \mathbf{0}_{3\times6}\right] \tag{20}$$

Finally, the measurement update is performed once again by following equations (16) and (17), but, in this case, measurements are given by the squared pseudorange $y_{\rho\,k} = \rho_k^2$, the observation matrix is $\boldsymbol{H}_{\rho\,k}$ and needs to evaluated at each iteration using Eq. (20). The measurement covariance is scalar and is denoted by $\boldsymbol{R}_\rho = \sigma_\rho^2$.

Error mitigation strategies Three error mitigation strategies have been proposed to deal with transmission delay, which affects GNSS measurements, ionospheric delay and clock biases, that affect pseudorange.

The first idea is that GNSS measurements have the same structure and the same dynamics as state variables. Hence, it is possible to use the filter's dynamics model to propagate an outdated measurement until the time at which it needs to be used for state update exploiting the fact that each GNSS measurement is time-tagged.

A clever solution to the clock bias problem can come from the availability of an ISL. In particular, by exploiting the properties of ranging measurements and the possibility of performing Dual One-Way Ranging, it is possible to compute a position estimate almost independent of clock biases and, in the meantime, obtain an estimate of the bias itself. It can be shown that the following combination of pseudorange measurements from S/C B to A and from A to B is independent of clock bias [4].

$$\rho_{\mathrm{DOWR}}(t) = \frac{\rho_{AB}(t) + \rho_{BA}(t)}{2} \tag{21}$$

The ionospheric interactions with pseudorange and carrier-phase measurements give rise to two opposite effects: group delay and phase advance. Since the contributions are equal in magnitude but opposite in sign, they vanish when summed. This feature has been exploited in the GRAPHIC (GRoup And PHase Ionospheric Correction) measurement, allowing an ionosphere-free range for single-frequency systems.

$$\rho_{\mathrm{GRAPHIC}} = \frac{1}{2}\left(\rho + \Phi\right) \tag{22}$$

5. Simulation framework

The adopted test scenario is taken from the VULCAIN mission. In particular, it features two identical 12U CubeSat flying in a trailing formation with an along-track separation of 150 km. The orbit is a circular $400 \times 400\ km$ SSO.
Ground-truth states are thus obtained by high-fidelity numerical propagation of the CubeSats trajectories, which are integrated separately. The orbital model includes 120^{th} degree EGM2008 spherical gravity, atmospheric drag, solar radiation pressure and third body attraction by Moon and Sun.
Measurements are simulated with the equations of Sec. 3, taking reasonable assumptions for the unknown coefficients. The GNSS receiver's performance data have been taken by the product sheet of the NovAtel OEM719 [5], a Commercial-Off-The-Shelf (COTS) receiver suitable for CubeSat applications.
Concerning pseudorange and carrier-phase simulation, the clock's parameters are those of the

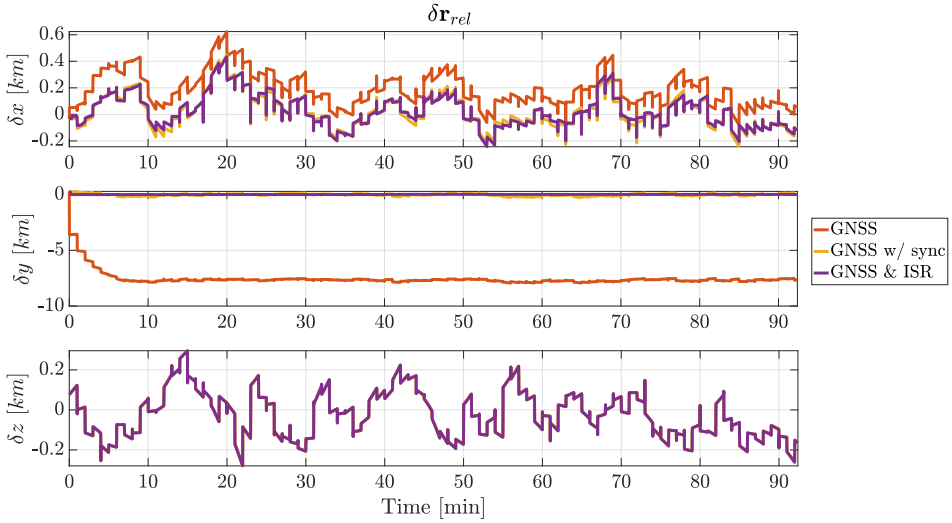

Figure 1: Relative position estimation error upgrades with different techniques.

CSAC clock, which is characterised by high stability and is suitable for CubeSat applications.

6. Results

The estimated states, both absolute and relative, are compared with the ground-truth ones. Since this work focuses on relative navigation, only the relative state estimation error for the relative position vector is here presented and discussed for different cases. This analysis is conducted considering the navigation filter running on spacecraft A, which receives delayed GNSS measurements from B.

In Fig. 1 is possible to assess the effect that each measurement has on the relative navigation accuracy. In particular, when using unsynchronized GNSS measurements (orange line), it is possible to notice that the use of delayed measurements introduces a bias in the along-track component of the relative position vector. This is compatible with the orbital description of the phenomenon. Being the leader in an along-track formation, if an *old* measurement is used to correct the position of spacecraft B, this latter will appear to be *behind* its actual position. The estimate of the relative position vector will thus be *shorter* than the true one, yielding a constant bias in the estimation error.
The effectiveness of the proposed synchronization technique is confirmed by the fact that the bias vanishes when enabled (yellow line).
Adding the ISR (purple line) impacts only the along-track component of the estimation error. This is confirmed by Fig. 2 where the nominal navigation scenario (i.e. the one with synchronized GNSS and pseudorange measurements) is reported. In particular, it is possible to notice how strongly the along-track covariance component benefits from the inter-satellite pseudorange. This can be easily explained since the inter-satellite position vector is always aligned with the along-track direction of the LVLH reference frame in the considered formation. The radial component is dynamically coupled with the along-track one and thus has a side benefit from δy improvements. Conversely, the out-of-plane component δz is uncoupled and is characterized by low observability. Thus, it is not affected by this measurement in any way.

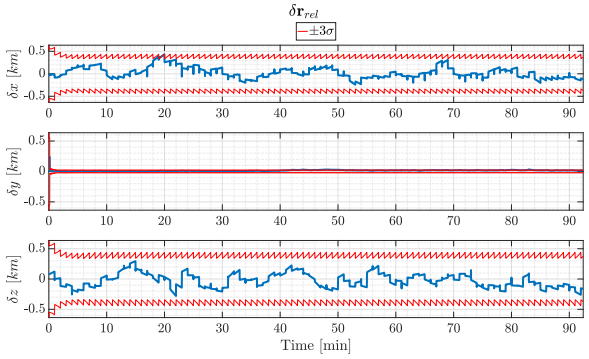

Figure 2: Relative position estimation error with GNSS, synchronization and inter-satellite pseudorange.

It is interesting to analyse the possibility of performing relative navigation with the inter-satellite pseudorange measurements only. This

could be the case of a contingency scenario, a deep-space mission, or any other situation in which GNSS-based solutions are unavailable.
The results are presented in Fig. 3. Surprisingly, a fair relative state convergence is maintained for the first two components of the relative position vector. Best results are obtained for the along-track component, as it is intuitive to understand considering the above-discussed geometrical reasons. The radial component benefits from being dynamically coupled with δy. Instead, the δz component, characterized by the lowest observability, diverges slightly after 30 minutes.

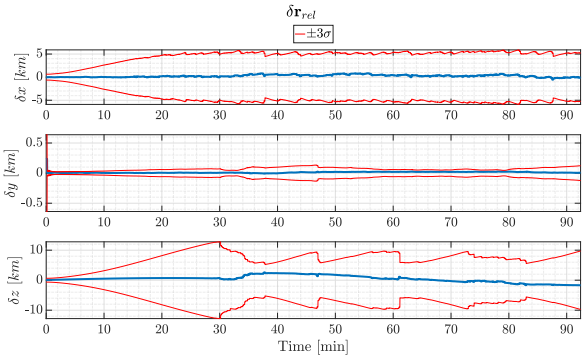

Figure 3: Relative position estimation error with inter-satellite pseudorange only.

7. Conclusions

In conclusion, concerning what has been addressed, it can be stated with resolution that an inter-satellite link in radio frequency can be actively exploited to perform relative navigation, whose accuracy depends on the chosen technique. In particular, the most important results of this study can be summarized as follows.
Based on the state of art, heritage and mathematical models of available ranging techniques, the feasibility of ISL-based relative navigation was established. To this end, it is necessary to establish a communication channel through an inter-satellite link between platforms.
The addition of a ranging measure to GNSS-based navigation turns out to be crucial in achieving higher accuracy in the relative state determination. It also enables increased system robustness in case of poor GNSS constellations geometry or unmodeled errors.
The stability of the onboard oscillator has proven to be a significant problem. It is, therefore, necessary to provide periodic clock corrections to counteract the vast positioning errors that this distortion would introduce in the long run. GNSS constellations can provide synchronization but are not always available. DOWR represents an excellent alternative method for clock synchronization independent from external systems.
Another major problem is the presence of delayed measurements in a filter architecture, which affects navigation accuracy. Therefore, appropriate strategies must be implemented to correct the distortions introduced by these delays. The one proposed in this thesis work has been shown to be effective for delayed GNSS measurements.
Finally, the possibility of performing ISR-only relative navigation in the considered spacecraft formation has been demonstrated. This result paves the way for more sophisticated relative navigation techniques independent of external systems, which will be critical for autonomous formation flight missions.

References

[1] R. Sun, J. Guo, D. Maessen, and E. Gill, "Enabling inter-satellite communication and ranging for small satellites," in *Proceedings of the 4S Symposium: Small Satelites, Systems and Services* (s.n., ed.), pp. 1–15, ESA, 2010. Small Satellites, Systems and Services - The 4S Symposium ; Conference date: 31-05-2010 Through 04-06-2010.

[2] M. L. Psiaki and S. Mohiuddin, "Modeling, analysis, and simulation of GPS carrier phase for spacecraft relative navigation," *Journal of Guidance, Control, and Dynamics*, vol. 30, pp. 1628–1639, Nov. 2007.

[3] L. Galleani, "A tutorial on the two-state model of the atomic clock noise," *Metrologia*, vol. 45, pp. S175–S182, Dec. 2008.

[4] J.-B. Thevenet and T. Grelier, "Formation flying radio-frequency metrology validation and performance: The PRISMA case," *Acta Astronautica*, vol. 82, pp. 2–15, Jan. 2013.

[5] NovAtel Inc., *NovAtel OEM 719 Product Sheet*, 7 ed., Apr. 2022.